Marine Geology 339 (2013) 13–21

Contents lists available at SciVerse ScienceDirect

Marine Geology

journal homepage: www.elsevier.com/locate/margeo

Evidence of mass failure in the Hess Deep Rift from multi-resolutional bathymetry data

Vicki Lynn Ferrini [a,*], Donna J. Shillington [a], Kathryn Gillis [b], Christopher J. MacLeod [c], Damon A.H. Teagle [d], Antony Morris [e], Pierre W. Cazenave [d], Stephen Hurst [f], Masako Tominaga [g], the JC21 Scientific Party

[a] Lamont-Doherty Earth Observatory of Columbia University, 61 Route 9W, Palisades, NY 10964, USA
[b] School of Earth and Ocean Sciences, University of Victoria, Victoria BC V8W 2Y2, Canada
[c] School of Earth & Ocean Sciences, Cardiff University, Park Place, Cardiff, CF10 3AT, United Kingdom
[d] National Oceanography Centre, University of Southampton Waterfront Campus, European Way, Southampton SO14 3ZH, United Kingdom
[e] University of Plymouth, Drake Circus, Plymouth, Devon, PL4 8AAm, United Kingdom
[f] Department of Geology, University of Illinois, 1301W. Green St., Urbana, IL 61801, USA
[g] Department of Geological Sciences, Michigan State University, 11 Natural Science, East Lansing, MI 48824, USA

ARTICLE INFO

Article history:
Received 21 March 2012
Received in revised form 15 March 2013
Accepted 26 March 2013
Available online 17 April 2013

Communicated by D.J.W. Piper

Keywords:
Hess Deep
Bathymetry
Mass failure

ABSTRACT

New regional swath and near-bottom bathymetric data provide constraints on shallow structures at the Hess Deep Rift, an oceanic rift that exposes the crust and upper mantle of fast-spreading oceanic lithosphere created at the East Pacific Rise. These data reveal the presence of a lobate structure with a length of ~4 km and a width of ~6 km south of an Intrarift Ridge, north of Hess Deep. The lobe consists of a series of concentric benches that are widest in the center of the lobe and narrower at the edges, with a dominant bench separating two distinct morphologic regions in the lobe. There are two end-member possible interpretations of this feature: 1) the lobate structure represents a mass failure with little translation that contains coherent blocks that preserve rift-related lineaments; or 2) it represents degraded tectonic structures, and the lobate form is accounted for by, for example, two intersecting faults. We favor the slump interpretation because it more readily accounts for the lobate form of the feature and the curved benches and based on the presence of other similar lobes in this region. In the slump model, secondary structures within the benches may indicate radial spreading during or after failure. The large lobate structure we identify south of the Intrarift Ridge in Hess Deep is one of the first features of its kind identified in an oceanic rift, and illustrates that mass failure may be a significant process in these settings, consistent with the recognition of their importance in mid-ocean ridges, oceanic islands, and continental rifts. Understanding the structure of the Hess Deep Rift is also important for reconstructing the section of fast-spreading oceanic crust exposed here.

1. Introduction

Morphologic evidence of submarine mass failure events is common along mid-ocean ridges, continental margins and near volcanic islands (e.g., Moore et al., 1989; Tucholke, 1992; McAdoo et al., 2000; Masson et al., 2002; Morgan et al., 2003), but to our knowledge, none have been documented in oceanic rifts. Many of the best-studied submarine landslides have been identified in sediment-dominated environments (e.g., McAdoo et al., 2000; Twichell et al., 2009), but evidence of submarine landslides has also been found in areas dominated by harder substrate (e.g., Moore et al., 1989; Tucholke et al., 1997). Mass failures in hard-rock environments exhibit a range of styles, but can be broadly classified either as deeply rooted slumps or debris avalanches (e.g., Varnes, 1978; Moore et al., 1989; Masson et al., 2002). The former often contain benches with tilted blocks indicating the rotation of cohesive substrate along a curved slip surface (e.g., Moore et al., 1989). They are not associated with significant translation and may happen gradually by creep. Conversely, debris avalanches are characterized by fields of blocks distributed over a large area and imply emplacement by a catastrophic event with large displacements (Masson et al., 2002; Morgan et al., 2003).

Understanding the processes associated with submarine mass failure and the resulting morphology is important for a number of reasons, including their possible causal association with tsunamigenesis (e.g., Tappin, 2010) and seismic activity (Eissler and Kanamori, 1987). Furthermore, submarine mass failures modify the architectures of the tectonic environments in which they form; thus to unravel the broader tectonic evolution of these systems, an understanding of the contribution of mass failure is also important.

A range of parameters is thought to control the propensity of an area to experience mass failure and the style of collapse that occurs.

* Corresponding author. Tel.: +1 845 365 8339; fax: +1 845 365 8179.
E-mail addresses: ferrini@ldeo.columbia.edu (V.L. Ferrini), djs@ldeo.columbia.edu (D.J. Shillington), kgillis@uvic.ca (K. Gillis), Macleod@cardiff.ac.uk (C.J. MacLeod), Damon.Teagle@southampton.ac.uk (D.A.H. Teagle), A.Morris@plymouth.ac.uk (A. Morris), pwc101@noc.soton.ac.uk (P.W. Cazenave), shurst@illinois.edu (S. Hurst).

0025-3227/$ – see front matter © 2013 Elsevier B.V. All rights reserved.
http://dx.doi.org/10.1016/j.margeo.2013.03.006

All of the hard-rock environments in which slumps are found are associated with the formation of steep topographic gradients due to faulting or volcanic construction, and mass wasting is commonly observed to degrade these structures (Tucholke et al., 1997). The occurrence and character of slumping will be further influenced by pre-existing tectonic and compositional structures. For example, some such slumps may be rooted in weak lithological layers (e.g., serpentinized peridotite), exploit tectonic faults, or be channeled by rugged fault-generated topography at the seafloor (Portner et al., 2011). Finally, slumping may be further triggered in tectonically active areas by earthquakes (Urgeles et al., 2006).

On submarine rifted margins mass failure has been documented during and/or immediately after continental rifting (e.g., Turner et al., 2008; Autin et al., 2010). In cases where the mass failure consists of a series of coherent blocks of crustal material or indurated pre-rift sediments and/or carbonates (e.g., a slump rather than a debris avalanche), there may be a continuum between extensional deformation and landsliding in terms of time-scales of motion and the architecture of the resulting rift. Likewise, mass failure by slumping or debris avalanches appears to be a regular process along volcanic islands and in mid-ocean ridges, modifying their morphology during and after magmatic and tectonic events (Bonatti et al., 1973; Tucholke et al., 1997; Morgan et al., 2003).

Oceanic rifts have received much less study, but mass failures may be equally important in modifying rift structure during and after tectonic extension and magmatism. Unraveling the contribution of mass failures in oceanic rifts is essential for a more comprehensive understanding of their tectonic and magmatic evolution. Here we present new data that reveal the surface morphologic characteristics of a lobate structure at the base of the Hess Deep Rift, which we interpret as evidence of a mass failure.

2. Hess Deep

The Hess Deep Rift lies at the tip of a rift propagating westward ahead of the intermediate-spreading (2.1 cm/yr half rate) Cocos-Nazca Ridge (Lonsdale, 1988; Floyd et al., 2001), and is presently ~30 km short of intersection with the East Pacific Rise (EPR) (Fig. 1). Several models have been proposed for the tectonic evolution of this region, including a single rotating microplate (Lonsdale, 1988), two counter-rotating microplates separated by Hess Deep (Klein et al., 2005) or a series of short lived rifts without significant rotation, which are controlled by stress associated with the Cocos-Nazca Rift and its distance from the EPR (Schouten et al., 2008). Although many extensional structures and much of the Cocos-Nazca Ridge strike roughly east–west, another set of features that strike ~055° is also present in Hess Deep (Lonsdale, 1988; Karson et al., 1992), and the westernmost tip of the Cocos-Nazca Ridge curves to the south (Fig. 1). Families of features with different orientations both within and around Hess Deep are likely related to the complex stress regime arising from the interaction of the EPR and Cocos-Nazca Ridge (Klein et al., 2005; Schouten et al., 2008; Smith et al., 2011).

The Hess Deep Rift is asymmetric; Hess Deep (5400 m depth) is flanked by a series of faulted blocks to the north, including the prominent Intrarift Ridge at 3000 m depth, and a comparatively simple scarp to the south (Fig. 2). Previous sampling with drilling, dredging and submersibles indicates that rocks from mid- to lower oceanic crust formed at the EPR are exposed immediately north of Hess Deep (e.g., Francheteau et al., 1990; Gillis et al., 1993; MacLeod et al., 1996), whereas the wall to the south of the deep is composed of outcrops of lavas and dikes, and rubble (Francheteau et al., 1990; Karson et al., 2002). ODP drilling at Hess Deep during Leg 147 sampled gabbros just below the dike-gabbro transition (Site 894, Fig. 2a) and cumulate gabbros and

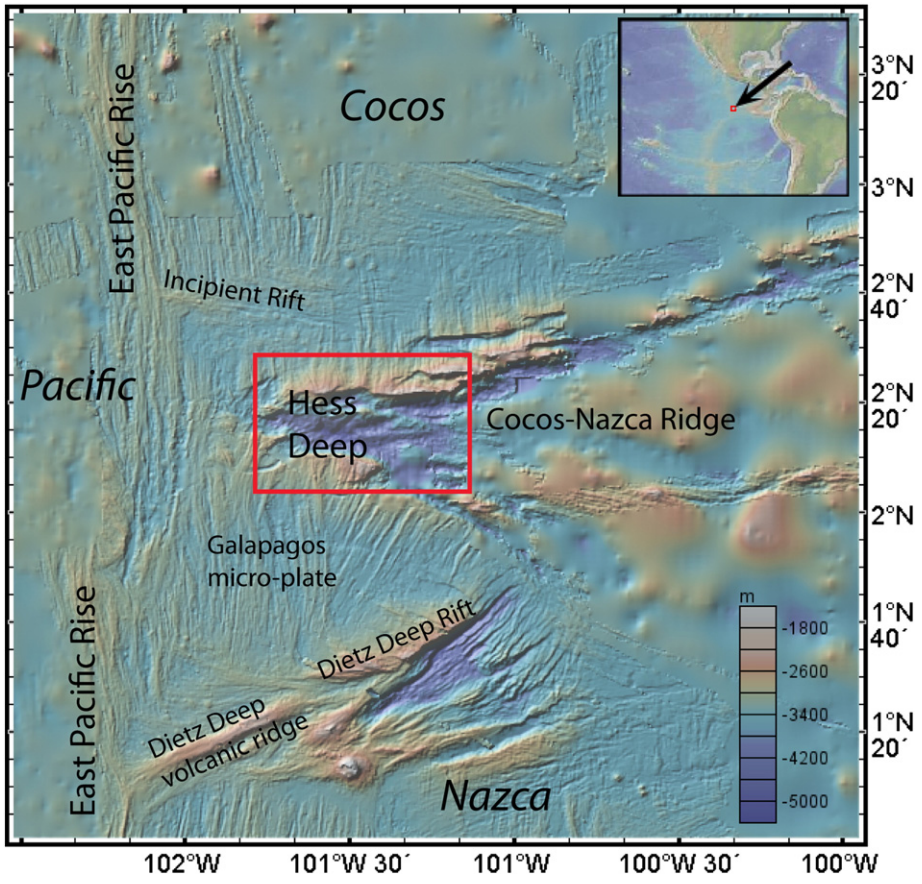

Fig 1. Regional bathymetry and tectonic setting of Hess Deep Rift (created with GeoMapApp). Red box identifies area shown in Fig 2. (For interpretation of the references to color in this figure legend, the reader is referred to the web version of this article.).

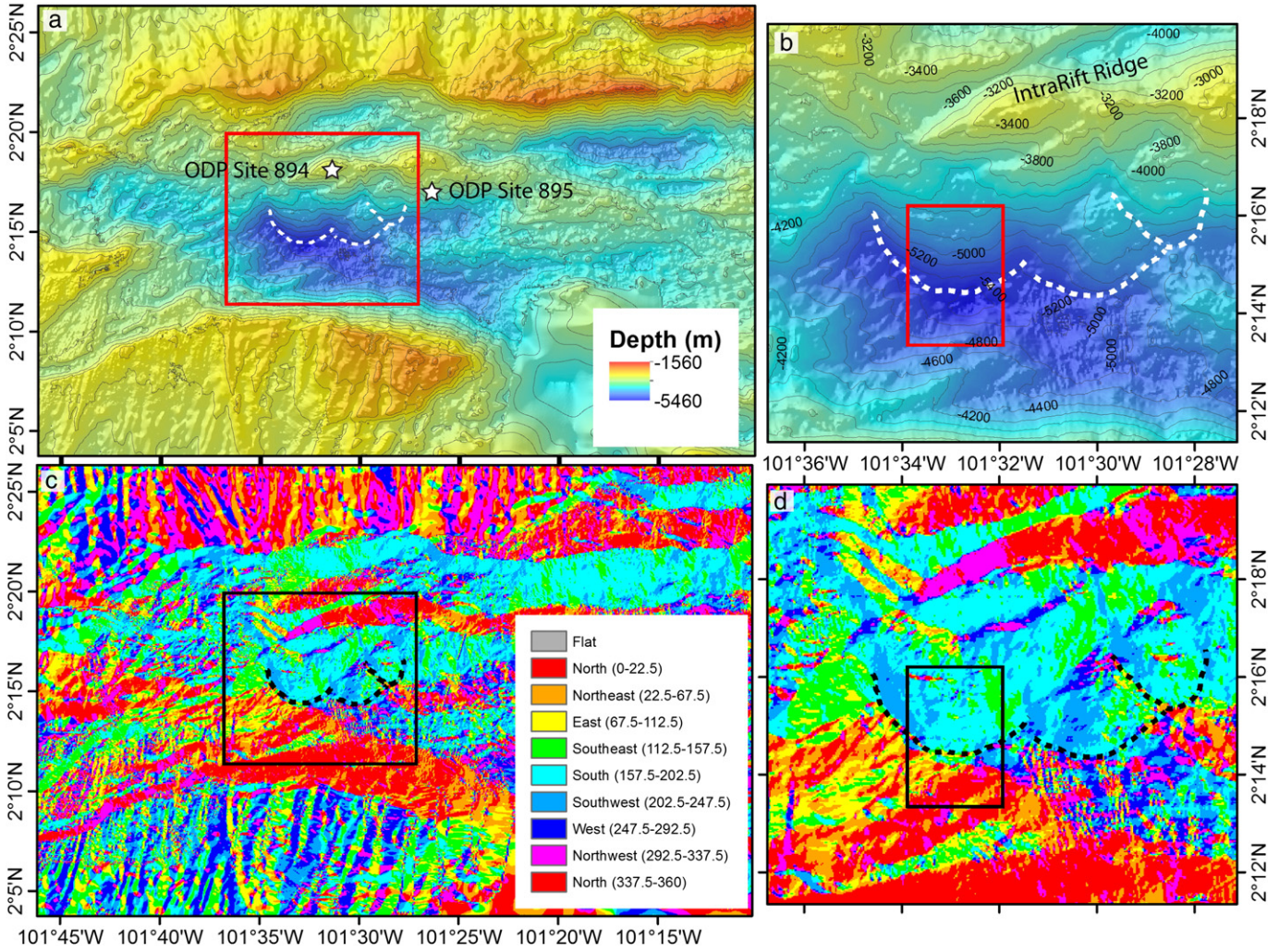

Fig 2. (a.) Gridded compilation of regional shipboard bathymetry data from the Hess Deep Rift including pre-existing data (Ryan et al., 2009) and new data from JC21 gridded at 50–100 m resolution with 200 m contours. Red box indicates the area of close-up shown in b. (b.) Close-up of regional shipboard bathymetry with 200 m contours. Area of near-bottom bathymetry survey (Fig. 3b) is indicated by red box. (c.) Seafloor aspect (directionality) of regional bathymetry, black box indicates close-up area in d. (d.) Close-up of seafloor aspect (directionality) focused on lobate feature, highlighting that the lobe itself interrupts the continuity of NE–SW trending features evident in this area. The N–S fabric associated with oceanic crust created at the EPR, and E–W and NE–SW structures associated with the Hess Deep Rift are evident in both bathymetry and seafloor aspect. Two additional lobate features are evident east of our near-bottom bathymetry survey area. (For interpretation of the references to color in this figure legend, the reader is referred to the web version of this article.).

mantle rocks around the crust–mantle boundary (Site 895) (Gillis et al., 1993).

3. Data acquisition and processing methods

In January–February 2008, a NERC/UK-IODP-funded cruise on the RRS *James Cook* (JC21) acquired shipboard and near-bottom bathymetric data in Hess Deep. Regional multibeam bathymetry data and subbottom profiler data were acquired using a hull-mounted Kongsberg Simrad EM120/SBP120 system (12 kHz) and processed with MB System (Caress and Chayes, 1995). They were gridded at resolutions varying from 50 to 150 m depending on the density of data coverage, with the smallest grid spacing in the area of focused study (red box, Fig. 2b). These data were combined with existing regional 100-m resolution bathymetry data available from the Marine Geoscience Data System using GeoMapApp (www.geomapapp.org; Ryan et al., 2009; Fig. 2). Subbottom profiler data was limited and mostly of very poor quality, so it was not used for this study except to provide a first-order estimate of sediment thickness on the dominant bench.

Near-bottom multibeam data were acquired along north–south survey lines at a nominal altitude of ~100 m, line spacing of ~200 m, and speed of 0.3 kts with a Simrad SM2000 (200 kHz) multibeam sonar system mounted on the ROV *Isis*. Swath widths during the *Isis* survey were ~200–350 m depending on noise and seabed characteristics (dip and reflectivity). *Isis* was navigated through the use of a high-precision Doppler Velocity Log (DVL) dead-reckoning navigational system that was geospatially constrained with Ultra-Short Base Line (USBL) navigation, and supplemented with a fiberoptic gyrocompass. Software tools developed through the U.S. National Deep Submergence Facility for processing precision navigation and sonar data (Roman and Singh, 2007; Ferrini et al., 2008) were used to create a high-quality self-consistent bathymetric grid. Bathymetry data were gridded at a resolution of 5 m using weighted mean gridding algorithm that employs a Gaussian basis function (Fig. 3b).

Geophysical data sets are supplemented with on-bottom ROV-based observations of the seafloor and are the focus of ongoing studies. Additionally, rock samples were collected from outcrops at the western end of the Intrarift Ridge and along its southern slope using Isis. Ongoing petrological and geochemical studies (e.g., MacLeod et al., 2008; Rioux et al., 2012; Lissenberg et al., 2013) provide constraints on the overall distribution of rock types needed to interpret the bathymetric features discussed in this paper. Overall, lithologies from increasingly deep sections of the crust are exposed towards the southeastern edge of the lobe. Evolved gabbros are found in the north and northwest section of

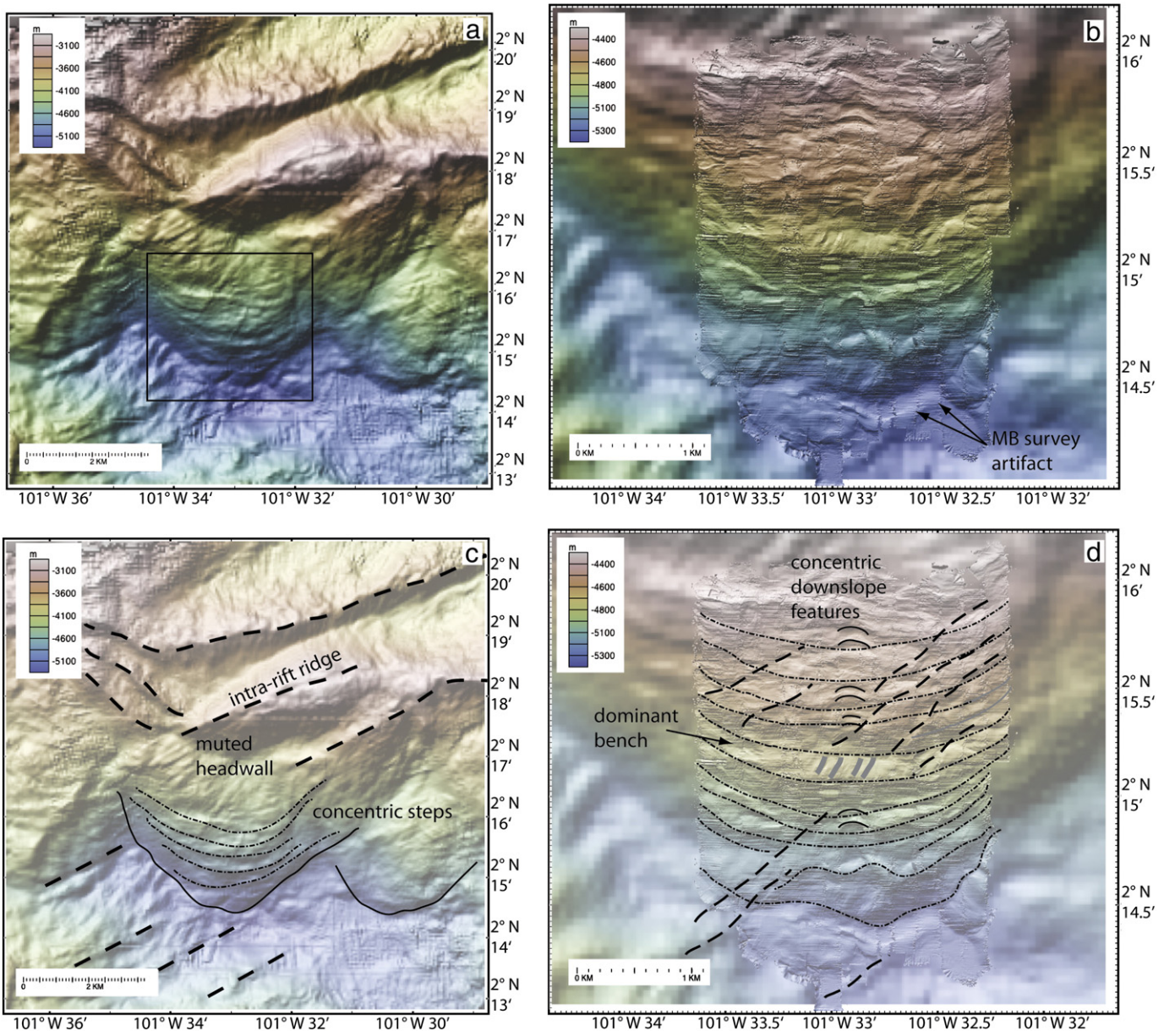

Fig 3. (Left panels) Regional swath bathymetry around interpreted slump illuminated from NW. The continuity of NE–SW trending linear structures (thick dashed lines) that roughly parallel the Intrarift Ridge, is interrupted by a clearly defined lobate structure. The lobe itself is characterized by a series of concentric rings (thin dashed lines) that are narrower near the edges, and wider near the center of the lobe. (Right panels) Additional structural details of the bathymetric steps are evident in the co-registered near-bottom bathymetry data (also illuminated from NW), and include benches and sub-benches (Ferrini et al., 2013). Superimposed on the dominant (widest) bench within the lobe are two sets of parallel linear structures. The E–W extent of these structures is spatially consistent with narrow concentric-downslope steps both upslope and downslope of the dominant bench. Note that multibeam survey artifacts are evident in the near-bottom bathymetry data as N–S seams between survey lines. Images made with GeoMapApp (www.geomapapp.org).

the survey and gabbros and peridotites are found towards the southeast. Dolerite samples were found throughout the lobe.

4. Observations

Shipboard bathymetry data reveal several faults and basement ridges within the Hess Deep Rift that are oriented roughly E–W, parallel to the overall trend of the rift valley (Figs. 2, 3a, b), consistent with earlier studies (Lonsdale, 1988). A secondary set of regional NE–SW-trending structures is also evident throughout the region with vertical relief of up to 0.5 km over horizontal scales of ~3 km. The N–S trending abyssal hill topography that parallels the East Pacific Rise is evident to the north and south of the rift valley (Fig. 2a, b). Shipboard bathymetry data also reveal three large lobate structures along the southern slope of the Intrarift Ridge (widths ~3–7.5 km, Fig. 2). Our near-bottom bathymetry survey was conducted over the largest of these lobes in an effort to image the structure and to guide bottom sampling between the Intrarift Ridge and Hess Deep.

The regional NE–SW trending linear structures that extend across the Hess Deep area are evident to the NE and SW of the large lobe, but their surface expression is interrupted by the lobe itself (Figs. 2c and 3a). A muted concave downslope feature within the southern flank of the Intrarift Ridge is located upslope of the lobe. It is defined by steeper gradients than the adjacent upslope regions (see 4400-m contour in Fig. 2b) with a relatively wide flat region immediately upslope of the lobe.

Within the lobe itself, concentric bathymetric benches (~200–500 m wide) that parallel bathymetric contours are visible in both the regional and near-bottom bathymetry (Fig. 3a, b). These benches are wider toward the middle of the lobe (~500 m), and narrower toward

the edges (~200 m). The lobe terminates abruptly at Hess Deep, and its downslope edge is bathymetrically distinct.

The near-bottom bathymetry data reveal additional details of the lobe including the presence of small benches and sub-benches toward the center of the lobe where the bathymetric steps are widest (Fig. 3b). The spacing between benches varies from ~50 to 400 m, and vertical offsets between them are as much as 200 m.

The near-bottom bathymetry data also reveal that the dominant bench at ~2° 15.167′N separates two distinct morphologic regions within the lobe, indicating structural differences (Fig. 3b). The benches in the upslope portion of the lobe are separated by relatively steep slopes (~30–40°), and are fairly continuous around the lobe. Downslope bathymetric profiles in this region, including the dominant bench, indicate that the benches have relatively flat tops, portions of which dip gently upslope (Figs. 4b, 5c, d). By contrast, downslope of the dominant slope, benches are less regular. Bathymetric profiles of this region indicate that benches are more rounded and less discrete (Fig. 5d). The observed differences in seafloor character relative to the dominant bench are consistent with ground-truth observations from ROV dives (MacLeod et al., 2008). Distinct outcrops interspersed with sedimented areas were observed above the bench, whereas the area below the bench was dominantly sedimented and contained fewer outcrops.

As described above, bathymetric benches exhibit variable structure across the lobe. They narrow toward the edges and exhibit internal structures toward the center of the lobe. The deepest region of the dominant bench is located near the lobe center, at depths of 4800–4850 m and appears to be covered by 10–20 m of sediment based on limited subbottom profiler data. Superimposed on this bench are two sets of N–S trending parallel ridges that are spaced ~20 m apart (Figs. 3c, 4a) and are associated with slopes up to ~29°. Small (~300-m-wide) concentric concave-downslope bathymetric steps with gently upslope-dipping bench tops are evident both upslope and downslope of the bench (Fig. 3b, d), and their extent is spatially consistent with the E–W extent of the parallel structures on the dominant bench.

Although the large regional NE–SW trending structures noted in regional bathymetry (Figs. 2c, 3a, c) are not directly identifiable within the lobate structure, the near-bottom bathymetry data reveal some smaller-scale localized linear features that appear to exhibit a similar trend (Fig. 3b, d); the apparent trends of features can be influenced by their intersection with the complex topography in this area. These features have <150 m relief over horizontal scales of up to 300 m (MacLeod et al., 2008), and are most clearly defined upslope of the dominant bench (Fig. 3b, d). Downslope of the dominant bench, however, these features are poorly defined at best, possibly because of the morphologic complexity of the benches near the toe of the lobe. The orientation of the apparent structural features on the dominant bench is slightly oblique (NNE–SSW) to these more regional trends (Fig. 3b, d).

5. Interpretation and discussion

5.1. Regional morphology of lobe

As described above, multi-resolutional bathymetry data characterize the morphology of a lobate feature in Hess Deep. In the upper portion of the lobe, benches are generally flat-topped and are separated by slopes of 30–40°, implying the presence of coherent blocks divided by normal separation faults (Figs. 3, 5d). By contrast, benches in the downslope

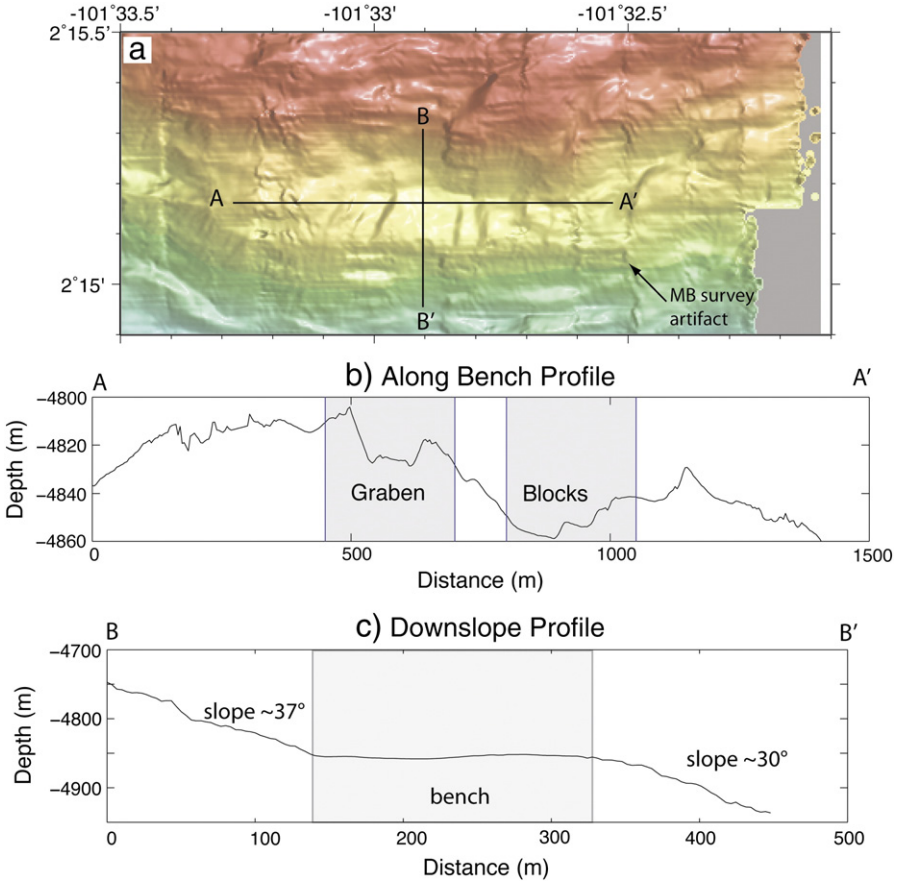

Fig 4. (a.) Close-up of near bathymetry on the dominant bench focused on parallel linear structures in the approximate center of the lobe. (b.) The across-bench profile reveals that the parallel linear features consist of a graben and fault blocks with slopes of up to ~29°. (c.) Downslope bathymetry profile showing that the dominant bench is flat-topped.

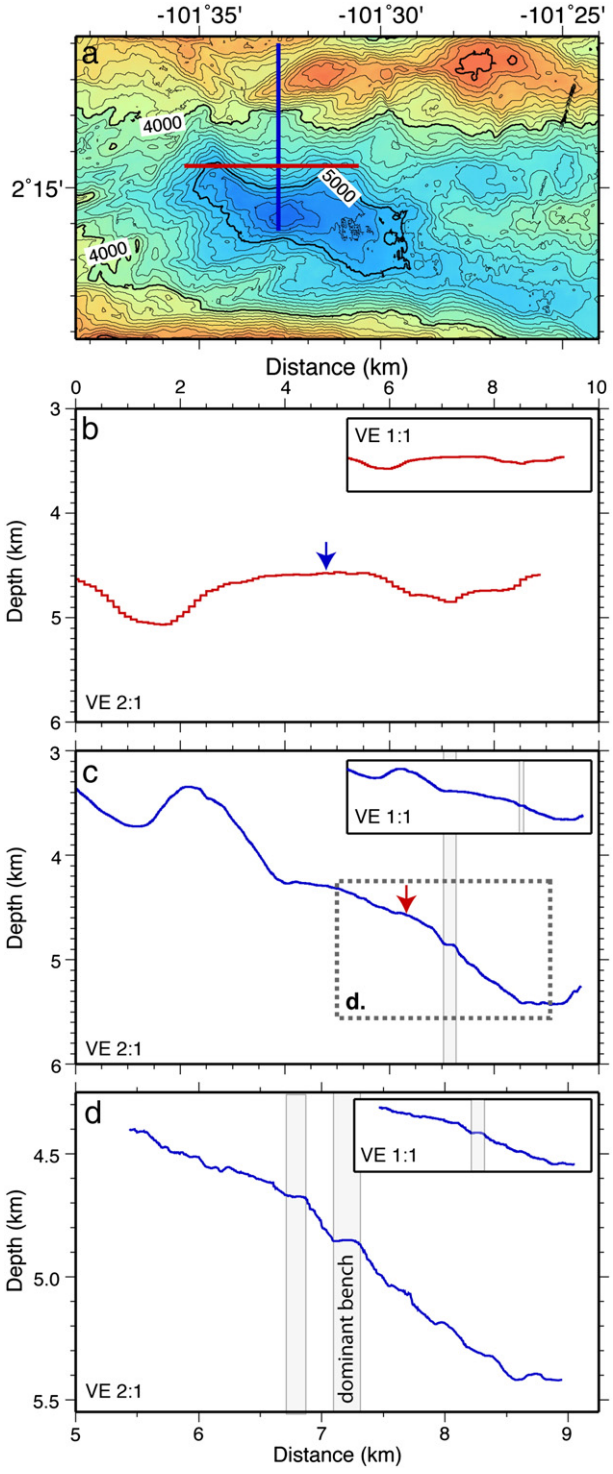

Fig 5. Bathymetric profiles of lobate feature in the Hess Deep Rift. (a.) Regional bathymetry compilation (50–100 m resolution) showing the location of profiles. (b.) Across-lobe profile of regional bathymetry from west to east focused on dominant bench. Arrow shows crossing point with profile in c. (c.) Downslope profile of regional bathymetry from north to south revealing both the muted headwall upslope of the lobe, and the dominant bench. Arrow shows crossing point with profile in b. (d.) Downslope profile of near-bottom bathymetry (5 m resolution) highlighting flat-topped benches.

portion of the lobe, particularly downslope of the dominant bench, are less continuous, have a more hummocky character, and terminate abruptly at the base of the lobe (Figs. 3, 5d). Any model for the formation of this feature must account for these characteristics.

5.2. Possible models for lobe formation: mass failure versus tectonics

We consider two end-member explanations for the morphologic characteristics of the lobate feature identified along the southern slope of the Intrarift Ridge: 1) the entire lobate structure may be a coherent slump, or 2) the feature be explained by a combination of tectonic structures and surficial mass failure structures. Although bathymetric data alone cannot definitively exclude either of these interpretations, we propose that the morphological characteristics favor the first interpretation, as described in greater detail below.

The overall lobate morphology and the consistent presence of superimposed concentric-upslope benches throughout the lobe support the interpretation of the entire lobe as a slump without significant translation. We observed different morphologies above and below a dominant bench in the center of the lobe; this change could result from extension in the upper portion that is balanced by compression in the lower portion. The fact that the lobe interrupts many regional structural trends (Figs. 2, 3) also implies that processes associated with the formation of this feature either post-date or were concurrent with the main rifting events, as described in more detail in Section 5.5. The flat-topped benches are a key indicator of the presence of hard underlying substrate as unconsolidated substrate would more likely have a hummocky character due to a lack of internal structural integrity.

The coherent blocks observed within the lobe suggest that the style of failure led to the preservation of some tectonic and compositional patterns. Observed patterns in lithology, while more complicated than those from previous sampling programs (Francheteau et al., 1990), reveal regional coherency (MacLeod et al., 2008; Rioux et al., 2012; Lissenberg et al., 2013), providing evidence that the overall stratigraphy of oceanic crust produced at the EPR is largely preserved by the style of slumping. In general, more evolved gabbros are observed towards the top (north-western part) of the lobe, while lithologies associated with deeper parts of the crust and upper mantle (layered gabbros and peridotites) are observed towards the base (south-eastern part) of the lobe. The small NE–SW features evident within the lobe that appear to parallel regional trends may have been formed after slumping and thus cross-cut the lobe, or may indicate that the style of slumping was such that some rift-related lineaments have been preserved; we favor the latter interpretation.

Morphologic characteristics of the lobe resemble submarine slumps in other submarine hard rock environments, such as mid-ocean ridges, the edges of volcanic islands and continental rifts. For example, landslides off Hawaii and the Canary Islands that are interpreted as slumps (rather than debris avalanches) appear to be cut by a series of evenly spaced faults, indicating that the slump comprises a few coherent blocks (Moore et al., 1989; Masson et al., 2002). They exhibit similar patterns of internal deformation, with series of normal separation faults in their upper portions and compressional toes at their bases. They are confined in their lateral extent, indicating that little translation has occurred. Similar structures are also observed on some mid-ocean ridges (Tucholke et al., 1997). Notably, the lobe in Hess Deep does not resemble hard-rock regions affected by debris avalanches, as observed at some volcanic islands (Moore et al., 1989) and mid-ocean ridges (Tucholke, 1992; Tucholke et al., 1997). Debris avalanches, by contrast, are characterized by chaotic deposits that span a large area.

The concave upslope shape of the upslope benches in Hess Deep differs from conceptual models for slumping, which have concave downslope features in their upper portions (Varnes, 1978). However, concave upslope features have been observed elsewhere (Moore et al., 1989). The overall concave upslope form of the benches on the lobe, the narrowing of benches from the center of the lobe towards its edges, and the structures within the dominant bench may all be partially explained by radial spreading of the slump during or subsequent to slumping. Small linear structures observed on the dominant bench are as steep as 29° and are unlikely to be sedimentary in origin since they

greatly exceed the angle of repose for sediments. Instead, they appear to be an isolated well-defined graben and an isolated set of fault blocks (Fig. 4b). These features are located within a bathymetric low near the center of the lobe, implying shallow localized internal structural failure within the consolidated substrate, which may be related to radial spreading of the failed material.

Alternatively, the lobate structure observed in Hess Deep could represent degraded tectonic structures overlain locally by thin mass wasting deposits. In this case, the benches with normal separation would represent normal faults formed by tectonics. A key challenge of this model is to account for the lobate form of this feature and the concavity of the benches. North and updip of the lobe, two basement features appear to that have NW–SE and NE–SW orientations (Fig. 2). One possible explanation is that the lobe represents a degraded version of these or other tectonic trends farther south into Hess Deep. Mass wasting in other settings, such as mid-ocean ridges, has been shown to modify and thus distort the apparent geometry of fault systems (Tucholke et al., 1997). Further, several mass wasting deposits in mid-ocean ridges have been documented at ridge-transform intersections or other areas of fault interaction (Daczko et al., 2005); these settings may be particularly susceptible to mass wasting.

In this model, the localized features within the bench could be the manifestation of shallowly west-dipping, north-striking features intersecting with the complicated topography in this region (rather than features formed during radial spreading of the lobe). We do not favor this interpretation due to the apparent lack of correlation between some of the features on the bench and corresponding NE–SW trending structures on the slope immediately above the bench.

We cannot differentiate between these two end-member explanations for the lobate structure in Hess Deep with the existing data. However, we favor the interpretation of the lobate feature as a slump because this model more readily accounts for the curved benches and lobate structure of this feature. Furthermore, there are other lobate structures in this rift observed in the regional bathymetry data (Fig. 2), suggesting that the topography created by the rift (and the exposed lithologies) may promote mass failure.

There is a continuum of hybrid models of these two end-member models for the formation of the lobe that may also be possible. Additional data including better imaging of subseafloor structures and an analysis of the distribution of lithologies are needed to differentiate between these two interpretations since a key difference is the manifestation of faults at depth. Faults formed by slumping will sole out onto a common failure surface, which reaches the surface at the top and base of the slump, whereas tectonic faults continue into the subsurface. However, based on the existing data, we favor the explanation of this feature as a coherent slump as described above.

5.3. Influence of pre-existing lithological and structural heterogeneity on the slump

Regardless of the exact mechanism of formation, it is clear that this feature is strongly influenced by the pre-existing tectonic and lithological template in this area. The Hess Deep Rift occurs in oceanic crust accreted at the East Pacific Rise. The dominate fabric created by this spreading center would be N–S and thus not favorably oriented to be reactivated by rifting or slumping since it is orthogonal to the rift and the interpreted slump. However, there may be other pre-existing structures that could have influenced later rifting and mass failure. For example, Lonsdale (1988) proposes that the formation of Hess Deep may have exploited a fracture zone created at the EPR. This or other pre-existing structures would clearly influence later extension and slumping. Structures created by rifting also likely controlled the style and location of slumping. Existing models propose that the architecture of the Hess Deep area (including the intrarift ridge) is formed by a combination of high-angle normal faulting and low-angle detachment faulting and/or by diapirism associated with serpentinization (Francheteau et al., 1990; MacLeod et al., 1996). Structures formed during rifting would also exert control on any later mass failures.

As described earlier, there appears to be an intersection of two large structures (one NE–SW trending, one NW–SE trending) upslope of the lobe (Fig. 2). The interaction of these two faults and degradation of their intersection might either explain the lobate shape of the feature in Hess Deep or have further promoted downslope instability. Mass failure features are observed in other places where faults intersect (e.g., ridge-transform intersections, Daczko et al., 2005); these regions may be particularly prone to mass failure.

Compositional heterogeneity may also have influenced the morphology of the lobe. Shipboard categorization of lithologies recovered during bottom sampling shows that progressively more primitive rocks are exposed towards the southeastern part of the lobe, with periodites found on the southeastern edge (see lithologies in Fig. 1 of Rioux et al., 2012). It is possible that the change in morphology of the lobe updip and downdip of the dominant bench may partially be explained by a broad change in lithology downslope. For example, serpentinite may be more abundant in the deeper, more mafic sections of the crust exposed towards the southeast, where there is more olivine. Serpentinite is weak (e.g., Escartin et al., 1997) and could partially account for the more hummocky, less coherent structures here.

However, there is not a correlation between lithological changes and the locations of benches. In other words, multiple lithologies were sampled along individual benches, and as a result, it does not appear that slumping exploited boundaries between lithological layers.

5.4. Causes for mass failure in Hess Deep

The faults as well as the gradients and orientations of slopes created by rifting during the formation of Hess Deep likely created conditions that could have promoted mass failure and strongly influenced its characteristics. Mass failure could have been additionally triggered by one or more discrete episodes of seismicity and/or diking, comparable to those observed in continental rifts (Wright et al., 2006), mid-ocean ridges (Tolstoy et al., 2006), and oceanic islands (Eissler and Kanamori, 1987). The large mass failure that we identify is located north of Hess Deep, to the west of the propagating tip of the Cocos-Nazca Ridge (Fig. 2), and is in an area that continues to experience active extensional deformation, as evidenced by ongoing seismicity concentrated in this region (Floyd et al., 2002). The base of the collapse is also unknown but may have exploited pre-existing zones of weakness within the EPR crust and/or faults formed during rifting, as described above. The presence of other lobate structures within Hess Deep (Fig. 2) implies that the steep gradients and pre-existing structures might promote mass failure over much of Hess Deep.

5.5. The timing and rate of mass failure

The temporal and spatial evolution of the proposed slump south of the Intrarift Ridge within the Hess Deep Rift is very poorly constrained. Since the continuity of regional features with NE–SW trends within the rift area is interrupted by the lobate structure, it is likely that slumping was either concurrent with or post-dated the processes that created the Intrarift Ridge and other large NE–SW regional structures. Slumps in mid-ocean ridges and continental rifts have been observed to occur both during active tectonism or afterwards (e.g., Tucholke et al., 1997; Autin et al., 2010). As described above, we interpret the presence of smaller structures paralleling these regional trends within the lobe is evidence that the style of slumping allowed some preservation of these features. An alternative explanation is that these structures cross cut the lobe and thus occurred after the formation of the lobe. This would support the idea that slumping occurred concurrently with rifting. On-bottom observations and limited sub-bottom profiler data indicate that a large portion of the lobe is covered in sediment

(~15 m in some areas), implying that slumping likely occurred some time ago.

Our observations allow for two possible end-member models for the temporal development of the slump at Hess Deep. In the first model, slumping occurred gradually, as inferred for slumps off Hawaii (Moore et al., 1989), with slow slumping accompanied by radial spreading that formed secondary structures within the benches. In the second model, the slump may have occurred relatively quickly, with a catastrophic failure followed by radial spreading of the deposited material. Although the interpreted slump in Hess Deep is not associated with a clear headwall, a muted amphitheater-shaped feature is located upslope of the lobe (Fig. 2). This may be evidence of a muted headwall of a slump that is not recent, but our data does not provide conclusive evidence of this. Alternatively, the slump in Hess Deep may lack a well-defined headwall if it occurred gradually instead of as a catastrophic event. Many slumps observed off volcanic islands are not associated with clear headwalls, perhaps owing to their slow, gradual formation (Moore et al., 1989).

5.6. The significance of mass failure in oceanic rifts

An important difference between our observations and similar features at other volcanic edifices is that this slump occurred in an oceanic rift. Several recent studies have highlighted the importance of mass failure at continental rifts and rifted margins. Some landslides clearly happen long after rifting and involve unlithified postrift sediments (McAdoo et al., 2000), but others may be an integral part of the rifting process. Synrift landslides can comprise coherent blocks of crustal material or indurated pre-rift sediments and/or carbonates that may have moved slowly, such that there is a continuum between extensional deformation and landsliding in terms of time-scales of motion and the architecture of the resulting rift. In some cases, mass failure may generate structures with unexpected orientations for a given stress field (e.g., perpendicular to opening direction offshore Iberia, Clark et al., 2007). However, because rifting commonly generates maximum slope gradients in the opening direction, material from the rift flanks often collapses into the rift depression (e.g., Turner et al., 2008; Autin et al., 2010). The base of the slump in continental rifts is thought to localize along a weak horizon within the pre-rift sediments or crust (Autin et al., 2010) or at the base of the crust (e.g., along serpentinized upper mantle (Clark et al., 2007)).

Likewise, previous studies also indicate that mass failure modifies the structure of mid-ocean ridges, both at the ridge axis and off-axis until fault scarps and other structures are buried by sediment (Tucholke et al., 1997). Slumping is strongly controlled by faults in this environment. The generation of steep topography is both a cause of mass failure and can channel the resulting slides and/or flows (Portner et al., 2011).

Our results indicate that mass failure may be an important process in oceanic rifts as well, and that they may be influenced by similar parameters. Oceanic rifts are the focus of significant study since they provide unique tectonic windows into the deep structure of intact oceanic crust. Hess Deep is a type location for studying fast spreading oceanic crust, and has been the focus of two drilling legs (Gillis et al., 1993, 2012), on-bottom sampling programs (Francheteau et al., 1990; MacLeod et al., 2008; Rioux et al., 2012; Lissenberg et al., 2013), and several geophysical experiments aimed at studying the structure of oceanic crust (e.g., Wiggins et al., 1996; Ballu et al., 1999; Christeson et al., 2007). Our results indicate that mass failure needs to be taken into account when reconstructing oceanic crustal structure in oceanic rift settings.

6. Conclusions

Near-bottom bathymetric data nested within shipboard swath bathymetry data reveal the presence of a 4 × 6 km lobate feature along the southern slope of the Intrarift Ridge at the Hess Deep Rift. The overall lobate form, concentric benches and interruption of regional tectonic trends by this feature support the interpretation of this feature as a slump. Although a number of recent studies have elucidated the importance of slumping in continental rifts, this is one of the first collapse features identified within an oceanic rift, demonstrating that mass failure is also an important process in these settings. Morphologic characteristics of this feature indicate that it is primarily composed of coherent blocks, such that rift-related structures and igneous stratigraphy of the EPR oceanic crust has been largely preserved. The concave upslope shape of benches and graben and fault blocks identified within the bathymetric low on the dominant bench further suggest radial spreading of the slumped material during or after failure.

Acknowledgments

We gratefully acknowledge the captain and crew of the RRS *James Cook*, and the ROV *Isis* team, who made the acquisition of these data possible. Data acquisition and shipboard analysis were funded by the UK Natural Environment Research Council grant NE/C509023/1 to CJM and DAHT as part of the UKIODP Site Survey Initiative, additional data analysis was supported by the US Scientific Support Program (USSSP) grant PDA0808 to DJS and VLF. Comments by Doug Masson, Bill Ryan, and Leslie Hsu, Ryan Portner and an anonymous reviewer greatly improved the manuscript.

References

Autin, J., Leroy, S., Beslier, M.-O., d'Acremont, E., Razin, P., Ribodetti, A., Bellahsen, N., Robin, C., Al Toubi, K., 2010. Continental break-up history of a deep magma-poor margin based on seismic reflection data (northeastern Gulf of Aden margin, offshore Oman). Geophysical Journal International 180 (2), 501–519. http://dx.doi.org/10.1111/j.1365-246X.2009.04424.x.

Ballu, V., et al., 1999. The density structure associated with oceanic crustal rifting at the Hess Deep: a seafloor and sea-surface gravity study. Earth and Planetary Science Letters 171, 21–34.

Bonatti, E., Honnorez, J., Gartner Jr., S., 1973. Sedimentary serpentinites from the Mid-Atlantic Ridge. Journal of Sedimentary Petrology 43, 728–735.

Caress, D.W., Chayes, D.N., 1995. New software for processing sidescan data from sidescan-capable multibeam sonars. Proceedings of the IEEE Oceans 95 Conference, pp. 997–1000.

Christeson, G.L., McIntosh, K.D., Karson, J.A., 2007. Inconsistent correlation of seismic layer 2a and lava layer thickness in oceanic crust. Nature 445, 418–421.

Clark, S.A., Sawyer, D.S., Austin Jr., J.A., Christeson, G.L., Nakamura, Y., 2007. Characterizing the Galicia Bank-Southern Iberia Abyssal Plain rifted margin segment boundary using multichannel seismic and ocean bottom seismometer data. Journal of Geophysical Research 112. http://dx.doi.org/10.1029/2006JB004581 (B03408).

Daczko, N.R., Mosher, S., Coffin, M.F., Meckel, T.A., 2005. Tectonic implications of fault-scarp-derived volcaniclastic deposits on Macquarie Island: sedimentation at a fossil ridge-transform intersection? GSA Bulletin 117, 18–31.

Eissler, H.K., Kanamori, H., 1987. A single-force model for the 1975 Kalapana, Hawaii, Earthquake. Journal of Geophysical Research 92, 4827–4836.

Escartin, J., Hirth, G., Evans, B., 1997. Effects of serpentinization on the lithospheric strength and the style of normal faulting at slow-spreading ridges. Earth and Planetary Science Letters 151, 181–189.

Ferrini, V.L., et al., 2008. Variable morphological expression of volcanic, tectonic, and hydrothermal processes at six hydrothermal vent fields in Lau Back-arc Basin. Geochemistry, Geophysics, Geosystems 9 (Issue Q07022, http://dx.doi.org/10.1029/2008GC002047).

Ferrini, V.L., et al., 2013. Near-bottom bathymetry data (2m resolution) from the Hess Deep Rift. IEDA, MGDS Data Collection. http://dx.doi.org/10.1594/IEDA/100267.

Floyd, J.S., et al., 2001. Evidence for fault weakness and fluid flow within an active low-angle normal fault. Nature 411, 779–783.

Floyd, J.S., Tolstoy, M., Mutter, J.C., Scholz, C.H., 2002. Seismotectonics of Mid-Ocean Ridge propagation in Hess Deep. Science 298, 1765–1768.

Francheteau, J., et al., 1990. 1 Ma East Pacific Rise oceanic crust and uppermost mantle exposed by rifting in Hess Deep (equatorial Pacific Ocean). Earth and Planetary Science Letters 101, 281–295.

Gillis, K.M., et al., 1993. Proc. ODP, Init. Repts., 147. Ocean Drilling Program, College Station, TX (366 pp.).

Gillis, K., Snow, J.E., Klaus, A., 2012. Hess Deep plutonic crust: exploring the plutonic crust at a fast-spreading ridge: new drilling at Hess Deep. Integrated Ocean Drillng Program Scientific Prospectus 345. http://dx.doi.org/10.2204/iodp.sp.345.2012.

Karson, J.A., et al., 1992. Tectonic Rotations of Dikes in Fast-spread Oceanic Crust.

Karson, J.A., et al., 2002. Structure of uppermost fast-spread oceanic crust exposed at the Hess Deep Rift: implications for subaxial processes at the East Pacific Rise. Geochemistry, Geophysics, Geosystems 3. http://dx.doi.org/10.1029/2001GC000155.

Klein, E.M., et al., 2005. Counter-rotating microplates at the Galapagos triple junction. Nature 433, 855–858.

Lissenberg, J., MacLeod, C.J., Howard, K.A., Godard, M., 2013. Pervasive reactive melt migration through fast-spreading lower oceanic crust (Hess Deep, equatorial Pacific Ocean). Earth and Planetary Science Letters 361, 436–447. http://dx.doi.org/10.1016/j.epsl.2012.11.012.

Lonsdale, P., 1988. Structural pattern of the Galapagos microplate and evolution of the Galapagos triple junctions. Journal of Geophysical Research 93 (13), 574.

MacLeod, C.J., Célérier, B., Früh-Green, G.L., Manning, C.E., 1996. Tectonics of Hess Deep: a synthesis of drilling results from Leg 147. In: Mével, C., Gillis, K.M., Allan, J.F., Meyer, P.S. (Eds.), Proc. ODP, Sci. Results, 147. Ocean Drilling Program, College Station, TX, pp. 461–475. http://dx.doi.org/10.2973/odp.proc.sr.147.032.1996.

MacLeod, C.J., et al., 2008. Cruise Report: "Accretion of the Lower Oceanic Crust at Fast-spreading Ridges: A Rock Drill and Near-bottom Seafloor Survey in Support of IODP Drilling in Hess Deep". Cardiff University.

Masson, D.G., Watts, A.B., Gee, M.J.R., Urgeles, R., Mitchell, N.C., Le Bas, T.P., Canals, M., 2002. Slope failure on the flanks of the western Canary Islands. Earth Science Reviews 57, 1–35.

McAdoo, B., Pratson, G., Orange, L.F., 2000. Submarine Landslide Geomorphology, U.S. Continental Slope. Marine Geology 169, 103–136. http://dx.doi.org/10.1016/S0025-3227(00)00050-5.

Moore, J.G., Clague, D.A., Holcomb, R.T., Lipman, P.W., Normark, W.R., Torresan, M.E., 1989. Prodigious Submarine Landslides on the Hawaiian Ridge. Journal of Geophysical Research 94 (B12), 17,465–417,484.

Morgan, J.K., Moore, G.F., Clague, D.A., 2003. Slope failure and volcanic spreading along the submarine south flank of Kilauea volcano, Hawaii. Journal of Geophysical Research 108 (B9), 2415. http://dx.doi.org/10.1029/2003JB002411.

Portner, R.A., Dickinson, J.A., Daczko, N.R., 2011. Interaction of gravity flows with a rugged mid-ocean ridge seafloor: an outcrop example from Macquarie Island. Journal of Sedimentary Research 81, 355–375.

Rioux, M., Lissenberg, C.J., McLean, N.M., Bowring, S.A., MacLeod, C.J., Hellebrand, E., Shimizu, N., 2012. Protracted growth scales of lower crustal growth at the fast-spreading East Pacific Rise. Nature Geoscience 5, 275–278. http://dx.doi.org/10.1038/ngeo1378.

Roman, C., Singh, H., 2007. A self-consistent bathymetric mapping algorithm. Journal of Field Robotics 24, 26–51. http://dx.doi.org/10.1003/rob.20164.

Ryan, W.B.F., et al., 2009. Global multi-resolution topography synthesis. Geochemistry, Geophysics, Geosystems 10, Q03014. http://dx.doi.org/10.1029/2008GC002332.

Schouten, H., Smith, D.K., Montési, L.G.J., Zhu, W., Klein, E.M., 2008. Cracking of lithosphere north of the Galapagos triple junction. Geology 36 (5), 339–342.

Smith, D.K., Schouten, H., Zhu, W.-l., Montési, L.G.J., Cann, J.R., 2011. Distributed deformation ahead of the Cocos-Nazca Rift at the Galapagos Triple Junction. Geochemistry, Geophysics, Geosystems 12. http://dx.doi.org/10.1029/2011GC003689.

Tappin, D.R., 2010. Submarine mass failures as tsunami sources: their climate control. Philosophical Transactions of the Royal Society 368 (1919), 2417–2434.

Tolstoy, M., Cowen, J.P., Baker, E.T., Fornari, D.J., Rubin, K.H., Shank, T.M., Waldhauser, F., Bohnenstiehl, D.R., Forsyth, D.W., Holmes, R.C., Love, B., Perfit, M.R., Weekly, R.T., Soule, S.A., Glazer, B., 2006. A sea-floor spreading event capture by seismometers. Science 314, 1920–1922.

Tucholke, B.E., 1992. Massive submarine rockslide in the rift-valley wall of the Mid-Atlantic Ridge. Geology 20 (2), 129–132. http://dx.doi.org/10.1130/0091-7613(1992)020<0129:MSRITR>2.3.CO;2.

Tucholke, B.E., Steward, W.K., Kleinrock, M.C., 1997. Long-term denudation of ocean crust in the central North Atlantic Ocean. Geology 25 (2), 171–174. http://dx.doi.org/10.1130/0091-7613(1997)025<071:LTDOC>2.3.CO;2.

Turner, J.P., Green, P.F., Holford, S.P., Lawrence, S.R., 2008. Thermal history of the Rio Muni (West Africa)-NE Brazil margins during continental breakup. Earth and Planetary Science Letters 270, 354–367.

Twichell, D.C., Chaytor, J.D., ten Brink, U.S., Buczkowski, B., 2009. Morphology of late Quaternary submarine landslides along the U.S. Atlantic continental margin. Marine Geology 265 (1–2), 4–15. http://dx.doi.org/10.1016/j.margeo.2009.01.009.

Urgeles, R., Leynaud, D., Lastras, G., Canals, M., Mienert, J., 2006. Back-analysis and failure mechanisms of a large submarine slide on the ebro slope, NW Mediterranean. Marine Geology 226, 185–206.

Varnes, D.J., 1978. Slope movement types and processes. Trans. Res. Board Special Report, 176, pp. 11–33.

Wiggins, S.M., et al., 1996. Hess Deep rift valley structure from seismic tomography. Journal of Geophysical Research 101, 22,335–322,353.

Wright, T.J., Ebinger, C., Biggs, J., Ayele, A., Yirgu, G., Keir, D., Stork, A., 2006. Magma-maintained rift segmentation at continental rupture in the 2005 Afar dyking episode. Nature 442, 291–294.